The Cryosphere Discuss., 8, 1831–1871, 2014
www.the-cryosphere-discuss.net/8/1831/2014/
doi:10.5194/tcd-8-1831-2014

The Cryosphere Discussions
Open Access

Sensitivity of CryoSat-2 Arctic sea-ice volume trends on radar-waveform interpretation

R. Ricker[1], S. Hendricks[1], V. Helm[1], H. Skourup[2], and M. Davidson[3]

[1]Alfred Wegener Institute, Helmholtz Centre for Polar and Marine Research, Bremerhaven, Germany
[2]DTU Space, Copenhagen, Denmark
[3]ESTEC, Noordwijk, the Netherlands

Received: 24 February 2014 – Accepted: 18 March 2014 – Published: 2 April 2014

Correspondence to: R. Ricker (robert.ricker@awi.de)

Published by Copernicus Publications on behalf of the European Geosciences Union.

Abstract

Several studies have shown that there is considerable evidence that the Arctic sea-ice is thinning during the last decades. When combined with the observed rapid reduction of ice-covered area this leads to a decline in sea-ice volume. The only remote sensing technique capable of quantifying this ice volume decrease at global scale is satellite altimetry. In this context the CryoSat-2 satellite was launched in 2010 and is equipped with the Ku-band SAR radar altimeter SIRAL, which we use to derive sea-ice freeboard defined as the height of the ice surface above the local sea level. In the context of quantifying Arctic ice-volume decrease at global scale, the CryoSat-2 satellite was launched in 2010 and is equipped with the Ku-band SAR radar altimeter SIRAL, which we use to derive sea-ice freeboard defined as the height of the ice surface above the sea level. Accurate CryoSat-2 range measurements over open water and the ice surface in the order of centimeters are necessary to achieve the required accuracy of the freeboard to thickness conversion. Besides uncertainties of the actual sea-surface height and limited knowledge of ice and snow properties, the penetration of the radar signal into the snow cover and therefore the interpretation of radar echoes is crucial. This has consequences in the selection of retracker algorithms which are used to track the main scattering horizon and assign a range estimate to each CryoSat measurement. In this paper we apply a retracker algorithm with thresholds of 40 %, 50 % and 80 % of the first maximum of radar echo power, spanning the range of values used in current literature. For the 40 % threshold we assume that the main scattering horizon lies at a certain depth between the surface and snow-ice interface as verified through coincident CryoSat-2 and airborne laser altimetry measurements. This contrasts with the 50 % and 80 % thresholds where we assume the ice-snow interface as the main scattering horizon similar to other published studies. Using the selected retrackers we evaluate the uncertainties of trends in sea-ice freeboard and higher level products that arise from the choice of the retracker threshold only, independently from the uncertainties related to snow and ice properties. Our study shows that the choice of retracker

TCD
8, 1831–1871, 2014

thresholds does have a non-negligible impact on magnitude estimates of sea-ice freeboard, thickness and volume, but that the main trends in these parameters are less affected. Specifically we find declines of Arctic sea-ice volume of 9.7 % (40 % threshold), 10.9 % (50 % threshold) and 6.9 % (80 % threshold) between March 2011 and March 2013. In contrast to that we find increases in Arctic sea-ice volume of 27.88 % (40 % threshold), 25.71 % (50 % threshold) and 32.65 % (80 % threshold) between November 2011 and November 2013. Furthermore we obtain a significant increase of freeboard from March 2013 to November 2013 in the area for multi-seasonal sea-ice north of Greenland and the Canadian Archipelago. Since this is unlikely it gives rise to the assumption that applying different retracker thresholds depending on seasonal properties of the snow load is necessary in the future.

1 Introduction

Sea-ice thickness is an important parameter of the polar cryosphere where changes in its seasonal cycle may cause significant negative feedback effects. There is already notable evidence for thinning of the Arctic sea-ice (Rothrock et al., 1999). Together with the rapid reduction of ice-covered area (Comiso et al., 2008), especially during the summer season (Stroeve et al., 2012), the reduction of sea-ice volume in the Arctic might exceed the rate of ice extent decrease. Therefore, long term observations of sea-ice volume are required to assess current changes of Arctic sea-ice thickness and its implications for a further reduction of the ice cover.

Basin-scale measurements of sea-ice thickness are currently carried out by satellite altimeter missions. The Altimetric sea-ice thickness retrieval is based on measurements of freeboard, the height of the ice-surface above the local water level, which can be used to calculate ice thickness (Kwok et al., 2009; Laxon et al., 2013). The radar altimeters onboard the ERS missions (Laxon et al., 2003) have been the first that were used for Arctic sea-ice thickness retrieval, followed by the EnviSat mission. These pulse-limited radar altimeters had a comparable large footprint of the order of

TCD
8, 1831–1871, 2014

10 km and an orbit coverage limited to 82.5° N. A better coverage up to 86° N was possible with the ICESat mission, which featured a laser altimeter with a significantly smaller footprint (70 m), but could be affected by clouds. The current satellite altimeter dedicated to Cryospheric science is CryoSat-2, which provides improved coverage of the Arctic up to 88° N.

CryoSat-2, a mission of the European Space Agency (ESA), was launched in April 2010 and is equipped with a Ku-Band radar altimeter (SIRAL – Synthetic Aperture Interferometric Radar Altimeter). Its range retrieval enables the calculation of the sea-ice freeboard, which is the height of the ice surface above the actual sea level. The sea-ice freeboard can be converted into sea-ice thickness, assuming hydrostatic equilibrium (Laxon et al., 2003; Wadhams et al., 1992). Therefore it is crucial to measure the main scattering horizon very accurately.

It has been suggested that Ku-Band radar waves do fully penetrate dry and cold snow (Beaven et al., 1995), however field experiments indicate that snow moisture and density layering may prevent a radar ranging through the snow to the ice surface in Arctic spring conditions over multi-year ice (Willatt et al., 2011).

The main scattering horizon is estimated at the leading edge of the radar echo waveforms. In synthetic aperture radar (SAR) altimetry, the waveform consists of a stack of collocated beams, separated from different bursts by their doppler informations. The main scattering horizon is obtained by a retracker algorithm, either an empirical threshold of the peak power or an empirical approximation of the entire waveform. Theoretical considerations of SAR altimetry suggests that the main scattering horizon is located near the peak power and not at the half power point on the leading edge as the case for conventional pulse-limited altimeters (Wingham et al., 2004). However, a variety of assumptions is used in literature. Laxon et al. (2013) used a half-power point while in a recent study dedicated waveform fitting results in an effective retracking near the waveform peak (Kurtz et al., 2014). In order to map land ice elevations Helm et al. (2014) again focused on the lower part of the leading edge to minimize spatial and temporal variations of the volume scattering contribution. The penetration

TCD
8, 1831–1871, 2014

of the main scattering horizon below the snow surface depends significantly on the choice of the threshold or the empirical waveform fitting method. Kurtz et al. (2014) found a mean difference of 12 cm between a 50 % threshold and a waveform fitting method with a near peak scattering horizon during the period 2011–2013. Therefore the choice of retracker adds to the existing uncertainty of physically limited penetration due to increased moisture or ice lenses in the snow layer. In addition, uncertainties arise due to variable footprint scale surface roughness and inaccurate reconstruction of the local sea-surface elevation.

The conversion of freeboard to sea-ice thickness again depends on the correct knowledge of snow depth and the densities of sea-ice and snow, all parameters not very well constrained by observations at basin-scale. First comparisons of CryoSat-2 sea-ice thickness data (Laxon et al., 2013) to validation data from airborne experiments and moorings show a good agreement on large scale, but scatter in the data comparison reflect the residual uncertainties cited above. Quantifying these uncertainties is essential for trend estimates in sea-ice and the use of CryoSat-2 data, for example in sea-ice modeling studies.

Here, we present CryoSat-2 freeboard and thickness retrievals with the first consistent uncertainty estimates in spring/autumn 2011, 2012 and 2013, using different approaches for waveform interpretation. We apply three different thresholds which span the range of values found in literature and access their impact on trends of CryoSat-2 Arctic sea-ice volume estimates. The goal of our study is to isolate and quantify the effect of SAR waveform interpretation from other uncertainties in the freeboard to thickness conversion. We describe the methodology and compare our findings to airborne datasets and other sea-ice remote sensing products. The contributions of different uncertainty sources are weighted and the total uncertainty is analyzed for its impact on observable Arctic sea-ice volume change relative to assumptions to the CryoSat-2 radar echo interpretation. We therefore investigate the effect of the retracker threshold range on the magnitude of Arctic sea-ice volume in spring and autumn, but also on the resulting trends.

TCD
8, 1831–1871, 2014

2 Data and methodology

2.1 Radar freeboard

The term sea-ice freeboard usually refers to the elevation of the snow/ice interface above the local sea level. With different altimetry sensor wavelengths we define the terminology of freeboard (Fig. 1):

1. The ice freeboard refers to sea-ice freeboard as defined above.
2. Snow freeboard: elevation of the air/snow interface, which is sensed by laser altimetry.
3. Radar freeboard: since the main scattering horizon may not be associated directly with the ice freeboard, we use the term radar freeboard for range measurements from CryoSat-2 (hereafter called CS-2). But lower wave propagation speed in the snow layer requires a correction based on assumed snow depth and penetration.

Figure 2 gives an outline of the steps in our data processing chain. To obtain radar freeboard it is necessary first to relate range estimates from the satellite to locate the main scattering surface. We use geolocated radar echoes provided by the ESA. Besides the SAR mode we also use data of SARIn mode for a defined area in the western Arctic Ocean and in coastal zones. SARIn data additionally contain phase information of the returning echo. Since they are not used in this study and to keep consistence, the phase information are discarded (Kurtz et al., 2014).

We obtain the two-way delay time of the averaged radar echoes (waveforms) by applying a TFMRA (Threshold-First-Maximum-Retracker-Algorithm) retracker (Helm et al., 2014). It involves an oversampling and a smoothing of the original waveform and determines the first maximum by derivative of the interpolated curve. In a second step the leading edge of the first maximum of the waveform is tracked at a certain threshold of the maximum power. We choose thresholds of 40 % (TFMRA40), 50 %

TCD
8, 1831–1871, 2014

(TFMRA50) and 80 % (TFMRA80) of the first-maximum power to simulate the assumptions in Helm et al. (2014), Laxon et al. (2013) and Kurtz et al. (2014). We assume that the resulting range gives the distance to the main scattering horizon. Figure 3 shows exemplary CS-2 waveforms for sea-ice and leads and the different applied thresholds. As a result we receive geolocated ellipsoidal elevations of CS-2 data for each orbit over sea-ice.

Second, the mean sea-surface height product DTU10 MSS (Andersen, 2010) is subtracted from the geo-located surface elevations to remove the main contributions of the actual sea-surface height. This is done to reduce errors in regions where the actual sea-surface cannot be obtained with sufficient accuracy.

Then, by applying a lead detection algorithm, we automatically obtain the actual elevation of the sea level in ice-free sections of the CS-2 ground tracks. Leads between ice floes usually have far less surface waves than the open ocean and thus feature a distinct mirror-like specular reflection. On the other hand diffusive radar returns over snow covered and roughened sea-ice surface lead to a wider angular distribution and a significantly different shape of the radar waveforms. Radar echoes over open ocean with higher significant wave height again show specific characteristics.

This surface-type dependance of radar waveforms is traditionally used to automatically classify leads in the ice pack (Laxon, 1994; Drinkwater, 1991). We consider several waveform parameters that are either available in the raw data files or can be computed from the waveforms. Table 1 gives an overview of these parameters and their assumed threshold values which are used to distinguish between the surface types "ocean", "lead" and "sea ice". We use the "pulse peakiness" PP that has already been described in Giles et al. (2008); Peacock and Laxon (2004). It has to be noted that we used a slightly different notation of the pulse peakiness in contrast to Laxon et al. (2013):

$$\mathrm{PP} = \sum_{i=1}^{N_{\mathrm{WF}}} \frac{\max(\mathrm{WF})}{\mathrm{WF}_i} \cdot N_{\mathrm{WF}} \tag{1}$$

TCD
8, 1831–1871, 2014

Here N_{WF} represents the number of range bins and WF_i the echo power at range bin index i. Thus PP can be transferred to values in Laxon et al. (2013) by a multiplication with a factor of $1/N_{WF}$. The second parameter is the "stack kurtosis" K which is a measure of peakiness of range integrated stack power distribution (Wingham et al., 2006). Here the term "stack" refers to an assembly of beam echoes which steer to a fixed point on the surface from different bursts. Specular reflections (narrow waveforms) from leads cause a high pulse peakiness as well as a small kurtosis. In contrast, echoes from sea-ice are defined by a wider shape and thus a lower peakiness. Further, the "standard deviation" SSD provides a measure of the variation in surface backscatter with incidence angle (Wingham et al., 2006). Off-nadir reflections from leads can bias the range retrieval, since the little area is required in the radar footprint to dominate the waveform. Because those echoes do not show the typical specular reflection they are refused by introducing a modified pulse peakiness which considers only three range bins on the "left" (PP_l) and on the "right" (PP_r) of the power maximum of a waveform:

$$PP_r = \frac{\max(WF)}{\mathrm{mean}([WF_{i_{max}-3}, WF_{i_{max}-1}])} \cdot 3 \quad (2)$$

$$PP_l = \frac{\max(WF)}{\mathrm{mean}([WF_{i_{max}+1}, WF_{i_{max}+3}])} \cdot 3 \quad (3)$$

For the coarse discrimination between ocean and sea-ice area (including leads) we use interpolated ice concentration from the daily OSI SAF ice concentration product (Eastwood, 2012). To identify echoes from the ocean we additionally consider the "OCOG WIDTH", which is derived from the algorithm of the OCOG retracker (Wingham et al., 1986). It provides information about the "width" of the echo. Surface waves on the ocean cause a high OCOG WIDTH which can be used for the surface type discrimination. Radar echoes that are not assigned to one of the surface types "ocean", "lead" or "sea ice" are assumed to be biased by off nadir leads and hence are discarded.

TCD
8, 1831–1871, 2014

2.1.1 Sea-surface anomaly

The surface-type classification parameters were initialized based on manual tuning of exemplary CS-2 ground tracks where coincident aircraft validation data (see Sect. 3) were available.The ranges of the retrieved open water spots from leads and ocean are interpolated and low-pass filtered over a 25 km window. This is done for each CS-2 track, yielding the sea-surface anomaly (SSA), the deviation of the actual sea-surface elevation from the mean sea-surface height (Fig. 1).

As the next step, the remaining anomaly from the mean sea-surface height (sea-surface anomaly SSA) that is obtained by the interpolated lead and ocean elevations is subtracted from the retracked surface elevations L, which were identified as sea-ice in the surface type discrimination. The radar freeboard F_R^*, which has not yet corrected for the lower wave propagation in the snow layer, is then yielded by:

$$F_R^* = L - (\mathrm{MSS} + \mathrm{SSA}) \tag{4}$$

2.1.2 Snow layer corrections

The effective scattering horizon of CS-2 range retrievals is the elevation that is obtained by the various retracker thresholds which have to be corrected for the lower wave propagation speed inside the snow layer. Thus we have to know the performance of the different thresholds to track the ice freeboard as well as the actual local snow depth. In general earlier studies assume that the effective scattering horizon is the ice freeboard for thresholds of 50 % (Laxon et al., 2013) and approximately 80 % (Kurtz et al., 2014). In this case the uncorrected radar freeboard F_R^* is obtained by a geometric correction for slower wave propagation speed in the full snow layer. Regarding Matzler and Wegmuller (1987), the correction can be applied by reducing the range below the snow/ice interface by the ratio of vacuum speed of light to local speed of light in the snow layer (22 % for a snow density of 300 $\mathrm{kg\,m^{-3}}$). If the main scattering horizon is located in the snow layer, either to the physical properties of the snow or due to the choice of

TCD
8, 1831–1871, 2014

a too low retracker threshold the snow propagation correction has to be reduced by the fraction of penetration into the snow layer accordingly.

We therefore parametrize the penetration P of the CS-2 range retrievals depending on different retracker thresholds and snow depths Z. The penetration is either the snow depth or a maximum penetration $P_{\max}$, depending on the retracker threshold. To make sure that the penetration does not exceed the snow depth in areas or regions with shallow snow cover, we limit $P_{\max}$ always to the local snow depth:

$$P(Z) = \begin{cases} Z & : Z < P_{\max} \\ P_{\max} & : Z > P_{\max} \end{cases} \tag{5}$$

We expect that $P_{\max}$ may vary with season and region for reasons of density layering but also decreased permittivity of wet snow. Thus $P_{\max}$ is a seasonal function, taking into account the winter season with rather cold, dry snow and the melting season with rather wet snow.

Finally, the actual radar freeboard F_R can be obtained by multiplying the uncorrected radar freeboard with a penetration correction factor for the wave propagation:

$$F_R = F_R^* + 0.28 \cdot P \tag{6}$$

We finally only allow freeboard values within the interval $0\,\text{m} < F_R < 2\,\text{m}$, since we assume that those values originate from insufficient retracking. For reasons of convenience and comparison to freeboard retrieval from laser altimetry (ICESat) we compute the snow freeboard for further conversion into sea-ice thickness:

$$F_S = F_R + P \tag{7}$$

TCD
8, 1831–1871, 2014

2.2 Sea-ice thickness

Snow freeboard F_S (Eq. 7) can be converted into sea-ice thickness T depending on the snow depth Z and the densities of snow (ρ_S), sea-ice (ρ_I) and sea water (ρ_W):

$$T = F_S \cdot \frac{\rho_W}{\rho_W - \rho_I} + Z \cdot \frac{\rho_S - \rho_W}{\rho_W - \rho_I} \quad (8)$$

Corresponding to Laxon et al. (2013), we use the Warren snow climatology (W99) for the estimation of snow depth (Warren et al., 1999) in the absence of year around snow-depth observations for the entire Arctic Ocean. The climatology is based on observations from drift stations in a period were the Arctic Ocean was dominated by multi-year sea-ice. It is therefore likely that the reduction of multi-year sea-ice in the recent decade (Nghiem et al., 2007) may have impacted the distribution of snow-depth in areas that are now more often covered by seasonal sea-ice. Based on data from an airborne snow-depth radar, Kurtz and Farrell (2011) suggest that though W99 is still representable for multi-year ice, but snow depth has to be reduced in first-year ice regions by 50 %. We follow this approach and classify the ice cover in first-year and multi-year sea-ice using the daily ice type product from OSI SAF (Eastwood, 2012) and apply the snow-depth reduction accordingly. This step was introduced by Laxon et al. (2013) for CS-2 data processing.

The snow density ρ_S is also taken from the Warren snow-water equivalent climatology (Warren et al., 1999). Both snow depths and snow density are available as a monthly product. We use ice densities ρ_I of 916.7 kg m^{-3} for first-year ice (FYI) and 882.0 kg m^{-3} for multi-year ice (MYI) (Alexandrov et al., 2010). Furthermore a value of 1024 kg m^{-3} is taken for the water density ρ_W.

The snow freeboard to thickness conversion is applied for each individual CS-2 ground track. We calculate ice thickness from an individual data point and not from a larger-scale averaged snow freeboard in order to allow estimation of individual uncertainties of retrieved thickness after later spatial downsampling. Only after that, data

TCD
8, 1831–1871, 2014

for one month are averaged on a EASE2.0 Grid (Brodzik et al., 2012) with a resolution of 25 km, including radar freeboard, snow depth, sea-ice thickness and all auxiliary data products. For averaging we use the arithmetic mean which is calculated from all processed data points within the boundaries of a grid cell. For sea-ice thickness, each grid cell represents the mean value of data points classified as sea-ice only, without the open water fraction.

2.3 Volume estimates

For the computation of sea-ice volume of the Arctic Basin we apply the ICESat/GLAS surface-type mask, but exclude the Baffin Bay (Fig. 4a) Fig. 4b shows the data mask and an exemplary monthly average snow depth field from November 2011, where the climatology shows consistently unrealistic snow depths in the excluded area.

In order to estimate the Arctic sea-ice volume we need to fill the gap of the CS-2 data retrieval above 88° N. Therefore we interpolate this region by applying a boxcar average of the width of 375 km (15 grid cells) to the thickness retrieval. The EASE2.0 grid is an equal area projection, therefore the monthly sea-ice volume V can be estimated as:

$$V = \sum_{j=1}^{M} c_j \cdot A \cdot \bar{T}_j \tag{9}$$

with the area A (625 km^2), the sea-ice concentration c_j and the monthly mean thickness $\bar{T}_j$ of grid cell j, added up over the total number M of grid cells. The sea-ice concentration c is a re-gridded product of the OSI SAF ice concentration that is used for CS-2 data processing along the CS-2 ground tracks.

2.4 Uncertainty of freeboard and thickness

Besides the uncertainty arising from the choice of the retracker thresholds, independent factors impact the accuracy of freeboard and thickness retrieval. In Wingham et al.

TCD
8, 1831–1871, 2014

(2006) different types of errors from CS-2 measurements over sea-ice have already been discussed. The first of which is the instrument system error that occurs as speckle noise and affects the range measurements. Second, there is an uncertainty of the reflection horizon depending on the physical properties of the snow cover. Third, the uncertainty of the actual sea level height (MSS + SSA), affects the freeboard retrieval through Eq. (6). Furthermore there are contributions which arise from uncertainties in densities of the sea-ice layer and snow loading, directly affecting the thickness retrieval through Eq. (8). Finally Wingham et al. (2006) consider potential high level errors due to limited recording of thin ice (< 1 m). However this was observed for pulse limited radar altimetry and is still not clarified for CS-2 (Laxon et al., 2013).

In this study we assume that these sources of uncertainty are independent of retracker thresholds and uncorrelated in general. Though we acknowledge that this is only a first order approximation resulting from incomplete knowledge of the covariance of individual error contributions.

The uncertainty of radar freeboard is assumed to be governed by the radar speckle and the accuracy of the actual sea surface height. The latter depends on the abundance of detected leads, which are needed for an accurate interpolation of the sea-surface anomaly.

Regarding Wingham et al. (2006), the estimated speckle noise originating from instrument system errors is between 0.10 m and 0.14 m, depending on the operating mode employed (SAR or SARin). In this study we therefore use a constant average value of $\sigma_{l1b} = 0.12$ m for this contribution. It affects the lead elevations as well as the ice floe elevations. The lead coverage is variable, depending on season, region and ice type. The SSA uncertainty σ_{SSA} is computed by taking the standard deviation of the detected lead elevations within a sliding 25 km window. In the absence of leads inside the moving window the uncertainty is given by the deviation of the mean SSA from the mean sea surface height MSS. As a consequence it rises with decreasing density of detected leads along a CS-2 ground track. We can then estimate the uncertainty of an

TCD
8, 1831–1871, 2014

individual radar freeboard measurement by adding the variances:

$$\sigma_{F_R}^2 = \sigma_{l1b}^2 + \sigma_{SSA}^2 \tag{10}$$

The uncertainty of sea-ice thickness σ_T for an individual measurement is then obtained by applying propagation of uncertainty to Eq. (8) (Giles et al., 2007):

$$\begin{aligned}\sigma_T^2 &= \left(\frac{\partial T}{\partial F_S}\cdot\sigma_{F_S}\right)^2 + \left(\frac{\partial T}{\partial \rho_S}\cdot\sigma_{\rho_Z}\right)^2 + \left(\frac{\partial T}{\partial \rho_I}\cdot\sigma_{\rho_I}\right)^2 + \left(\frac{\partial T}{\partial Z}\cdot\sigma_Z\right)^2 \\ &= \left(\frac{\rho_W}{\rho_W-\rho_I}\right)^2\cdot\left(\sigma_P^2+\sigma_{F_R}^2\right) + \\ &\quad \left(\frac{Z}{\rho_W-\rho_I}\right)^2\cdot\sigma_{\rho_Z}^2 + \\ &\quad \left(\frac{F_S\cdot\rho_W+(\rho_S-\rho_W)\cdot Z}{(\rho_W-\rho_I)^2}\right)^2\cdot\sigma_{\rho_I}^2 + \\ &\quad \left(\frac{\rho_S-\rho_W}{\rho_W-\rho_I}\right)^2\cdot\sigma_Z^2\end{aligned} \tag{11}$$

using uncertainties for radar freeboard (σ_{F_R}), snow depth (σ_Z), ice density (σ_{ρ_I}) and snow density (σ_{ρ_Z}). For an uncertainty estimation of the sea-ice thickness we have to include the uncertainty σ_P that results from the potential radar penetration. Considering comparisons between airborne laser and CS-2 radar altimeter measurements (Sect. 3), we assume an arctic wide uncertainty of 0.1 m. The contribution of errors due to the variability of water density are neglected (Kurtz et al., 2012). Table 2 summarizes the contributions to the freeboard and thickness uncertainty estimates.

Due to monthly averaging the uncertainties of the individual measurements are reduced, leading to the variance of grid cell of monthly mean freeboard and thickness

TCD
8, 1831–1871, 2014

respectively :

$$\sigma^2_{\bar{F},\bar{T}} = \frac{\sum_{i=1}^{N} \sigma^2_{F_i,T_i}}{N^2} \tag{12}$$

with variances $\sigma^2_{F_i,T_i}$ of individual freeboard and thickness measurements and N, the number of measurements within a grid cell. Considering Eq. (9) and assuming a sea-ice concentration uncertainty $\sigma_{c_j} = 0.05$ for each grid cell, the Arctic sea-ice volume uncertainty σ_V is obtained by:

$$\begin{aligned}\sigma^2_V &= \left(\frac{\partial V}{\partial c_j} \cdot \sigma_{c_j}\right)^2 + \left(\frac{\partial V}{\partial \bar{T}_j} \cdot \sigma_{\bar{T}_j}\right)^2 \\ &= \sum_{j=1}^{M} V_j^2 \cdot \left(\left(\frac{\sigma_{c_j}}{c_j}\right)^2 + \left(\frac{\sigma_{\bar{T}_j}}{\bar{T}_j}\right)^2\right)\end{aligned} \tag{13}$$

where the uncertainties of each grid cell are added up over the total number M of grid cells.

3 Airborne validation

In contrast to the thresholds of TFMRA50 and TFMRA80 where we assume the ice freeboard as the main scattering horizon, we have to determine the signal penetration into the snow layer when applying the TFMRA40 retracker. Since laser altimetry is always referring to the snow freeboard we can accomplish that by comparing airborne laser altimeter data to collocated CS-2 measurements.

Since 2005 the CryoSat Validation Experiment (CryoVex) is carried out over sea-ice in the Northern Hemisphere to directly validate CS-2 products. During the CryoVEx campaign in the Lincoln Sea in spring 2011 the first coincident measurements by CS-2

TCD
8, 1831–1871, 2014
CryoSat-2
R. Ricker et al.

and two research aircraft were accomplished. Besides other sensors a laser scanner was mounted on board of the AWI aircraft “Polar 5”.

Airborne laser scanner (ALS) provide high-precision and high-resolution measurements and thus are capable to evaluate measurements of the radar altimeter SIRAL on CryoSat-2. The accuracy for the range measurements is about a few cm. The main limitation is due to GPS positioning, especially for a longer baseline of more than 100 km (Forsberg et al., 2002).

The laser scanner has been operated at an altitude of 300 m with around 370 shot points each scan line and a point spacing of around 0.3 m. The spacing along track has been around 1 m. Into our analysis we include two flights where we consider profile sections with a total length of about 450 km in coincidence with CS-2. They took place on 15 and 17 April and were operated from the Canadian Forces Station Alert (Fig. 5a).

In consistence with the CS-2 processing the geolocated ALS elevations have to be referenced to the actual sea surface height. Therefore leads are picked manually out of the ALS elevation model. The sea-surface height is then determined along the center shot points by applying a spline interpolation. The snow freeboard is then obtained by subtracting the sea-surface height from the geolocated ALS elevations.

In order to provide a consistent comparison with CS-2 measurements the ALS data points are weighted, depending on the distance to the respective CS-2 data point, that we assume to be located in the center of the CS-2 Doppler cell. In the following step the ALS data are averaged over the respective CS-2 Doppler cell, which is assumed to cover an area of 300 m by 1000 m. The averaging process is applied to accommodate the footprint geometry and therefore the coarser resolution of CS-2 measurements. Finally every averaged value of the ALS data is assigned to a corresponding CS-2 data point.

Figure 5 shows ALS snow freeboard and CS-2 uncorrected radar freeboard F_R^* (Eq. 4) in a direct comparison, for which only valid data from coincident coverage are considered. Gaps in Fig. 5b originate from discarded CS-2 data that were biased by off-nadir leads or insufficient retracking and poor quality in the ALS data. Furthermore

TCD
8, 1831–1871, 2014

we additionally smoothed both data sets with a boxcar average of 10 km width for a better contrast. The along track comparison in Fig. 5 shows some long scale agreement of the freeboard gradient, exemplary between 150 and 200 km track distance on ground track 5428. In general we observe an offset between snow and radar freeboard. This is also shown in the corresponding probability density functions in Fig. 5c. Here we use a relative probability that reveals the modal freeboard as the peak of the function which represents the level ice. The tail represents the fraction of deformed ice. As deviation between the mean snow (ALS) and radar (CS-2) freeboard we receive 0.18 m along track 5399 and 0.27 m along track 5428.

The offset that we can observe in Fig. 5 results from the apparent penetration of the radar into the snow layer. To determine the penetration depth we average the mean differences between ALS and CS-2 and obtain 0.225 m. Since we consider the uncorrected radar freeboard F_R^* we hence obtain the apparent penetration that also has to be corrected for slower wave propagation in snow to get the actual penetration. Reducing the apparent penetration by 22 % yields an actual penetration of 0.18 m.

From simultaneous in-situ measurements on the ground we additionally know that the mean snow depth exceeded 0.3 m. Therefore it is also clear that regarding the TFMRA40 retracker the radar does not penetrate the snow cover to the ice/snow interface. However we note that this comparison might be only valid for the multi-year ice region north of Alert in spring.

4 Results

4.1 Radar freeboard retrieval

Figure 6a shows the CS-2 mean radar freeboard retrieval from April 2011 using the TFMRA40 retracker threshold. For the penetration parametrization (Eq. 5) of the entire Arctic we used the value P_{max} = 0.18 m, that resulted from the direct comparison of CS-2 and validation measurements (Sect. 3). We find a mean radar freeboard of 0.33 m in

TCD
8, 1831–1871, 2014

the multi-year ice (MYI) region north of Greenland and the Canadian Archipelago and mean radar freeboard of 0.21 m for seasonal ice (FYI). For the discrimination between FYI and MYI we use a monthly mean ice-type product. During the CS-2 data processing OSI SAF ice-type data are interpolated along each CS-2 ground track. As for the CS-2 freeboard and thickness retrieval the interpolated ice-type data are averaged on the EASE2.0 grid over one month.

The corresponding map of radar freeboard uncertainties (Fig. 6b) shows a latitude-dependent gradient. The mean uncertainties for FYI and MYI do not differ significantly and are around 0.03 m. Increased uncertainties of up to 0.1 m can be observed in the Canadian Archipelago and land-fast ice regions like the Laptev Sea (black dashed circle).

Figure 6c shows a monthly mean of MESOP ASCAT Backscatter from April 2011. High backscatter indicates a rather rough surface and hence MYI, whereas low backscatter rather indicates younger FYI. A slightly Increased freeboard can be observed in the East Siberian Sea. It occurs as higher backscatter in Fig. 6c (black dashed square), though here this region is slightly shifted to the west.

Figure 6d shows the lead detection map of April 2011. It illustrates the percentage of leads within one grid cell as a fraction of lead-flagged waveforms of the total number of CS-2 measurements. Fractions of up to 15 % can be found in the Barents and Kara Sea east of Svalbard. We also note low lead fractions of < 1 % in land-fast ice regions like the Laptev Sea (black dashed circle).

4.2 Freeboard, thickness and volume retrievals from different retracker thresholds

Figure 7 shows the radar freeboard from March and November 2013 together with the corresponding uncertainty maps, retrieved by applying different thresholds (40 %, 50 % and 80 %) for the TFMRA retracker. Table 3 summarizes the corresponding mean values classified into FYI and MYI. Considering the results of the TFMRA40 retracker we find a mean radar freeboard of 0.17/0.3 m of FYI/MYI in March and 0.11/0.31 m

TCD
8, 1831–1871, 2014

of FYI/MYI in November. However in contrast to March the November retrieval shows increased radar freeboard north of Greenland and the Canadian Archipelago. The corresponding uncertainties generally show an increase from March to November.

For the TFMRA50 and TFMRA80 retrievals we assume that the ice/snow interface is the main scattering horizon. In this case the radar freeboard is equal to the ice freeboard and the radar penetration is equal to the full snow depth. In comparison to the TFMRA40 the TFMRA50 radar freeboard is slightly decreased, but shows similar patterns, in particular the shape of the MYI region. The deviation to TFMRA40 is −0.03/ − 0.02 m for FYI/MYI in March 2013 and −0.02/ − 0.05 m for FYI/MYI in November 2013. The TFMRA50 uncertainties are in the order of the TFMRA40 retrieval and show the same pattern.

We find a significant decrease of radar freeboard of TFMRA80 in comparison to the TFMRA40 and TFMRA50 retrievals. Between TFMRA80 and TFMRA40 we find deviations of −0.08/ − 0.12 m for FYI/MYI in March and −0.05/ − 0.16 m for FYI/MYI in November. Furthermore the TFMRA80 uncertainty map shows increased values in comparison to the TFMRA40 and TFMRA50 retrievals while the general pattern remains.

In conformance to Fig. 6 the uncertainties of all products show increased values in the land-fast ice region of the Laptev Sea as well as a latitude-dependent gradient.

Figure 8 shows the sea-ice thickness from March and November 2013 together with the corresponding uncertainty maps. Areas where the climatology shows consistently unrealistic snow depths were excluded by the data mask (Fig. 4). The TFMRA40 retrieval reveals a mean sea-ice thickness of 1.97/2.1 m in March 2013 and 1.25/2.22 m in November 2013. The contrast between the MYI region north of Greenland and FYI is rather low, especially in March.

The TFMRA50 retrieval shows a higher contrast between MYI and FYI than it can be observed in the TFMRA40 retrieval. The uncertainty map for both products shows the same features again. In comparison to the corresponding freeboard retrievals the thickness uncertainties are increased by a factor of around 10. Again we find high

TCD
8, 1831–1871, 2014

uncertainties in land-fast ice regions and a latitude dependent gradient. The deviations for FYI/MYI between TFMRA50 and TFMRA40 are −0.26/0.64 m in March 2013 and −0.23/0.12 m in November 2013. Conforming to Fig. 7 the TFMRA80 retrieval shows decreased sea-ice thickness compared to TFMRA50 and TFMRA40. Further we find deviations of −0.81/ − 0.22 m for FYI/MYI in March and −0.61/ − 0.79 m for FYI/MYI in November between the TFMRA80 and TFMRA40 retrievals.

Figure 9 shows the Arctic sea-ice volume estimates and corresponding uncertainties for March and November 2011, 2012 and 2013. They are discriminated regarding the chosen retracker threshold and the ice type. The total volumes of TFMRA40 and TFMRA50 are very close and differ by less than 0.5×10^3 km^3. On the other hand the ratio between FYI and MYI is significantly different. For TFMRA40 the fraction of FYI volume is always higher than in both TFMRA50 and TFMRA80. We also note that the total volume of the TFMRA80 is significantly lower than the other retrievals and never exceeds 10×10^3 km^3.

Table 4 summarizes the volume estimates and the deviations relatively to the 2011 retrievals. For the TFMRA40 volume estimates we find a decline of $1.57 \pm 4.58 \times 10^3$ km^3 between March 2011 and 2013 while for November we observe an increase of $2.52 \pm 4.11 \times 10^3$ km^3. For TFMRA50 and TFMRA80 we find gradients with the same leading sign but of different magnitudes. For TFMRA50 we observe a decline of $1.69 \pm 4.82 \times 10^3$ km^3 between March 2011 and 2013 and an increase of $2.62 \pm 4.28 \times 10^3$ km^3 for November and further a decline of $0.73 \pm 5.51 \times 10^3$ km^3 between March 2011 and 2013 and an increase of $1.7 \pm 4.79 \times 10^3$ km^3 for November. The uncertainties of the total sea-ice volume vary between 2 and 3×10^3 km^3, not including the choice of the retracker threshold.

5 Discussion

The comparison of the regional distribution of the example CS-2 freeboard maps of April 2011 with ASCAT backscatter data shows similar geographical features. Since

TCD
8, 1831–1871, 2014

MYI is usually associated with higher ASCAT backscatter both backscatter and freeboard should correlate. Local features like a small area of potentially MYI in the Siberian sea are visible (black dashed box in Fig. 6a) in both datasets and give confidence that CS-2 is indeed able to capture actual distribution of sea-ice types. Other similarities can be seen in the lead detection map in the Barents and Kara Sea, where higher ASCAT backscatter in a young FYI region coincides with higher fraction of detected leads. The discussion of the physical relationship is beyond the scope of this paper, but it should be investigated in more detail for a potential improved lead detection and freeboard retrieval in thin ice areas.

Besides the freeboard and thickness data, we also calculated a first order estimation of their uncertainties. The latitude dependent gradient results from the higher number of measurements within a 25 km × 25 km grid cell. A higher number of measurements reduces the uncertainty of each grid cell (Eq. 12), therefore orbit patterns may arise from the slightly different numbers of data points per grid cell and thus affect $\sigma^2_{\bar{F},\bar{T}}$. Increased uncertainties appear in land-fast ice regions like the Laptev Sea because of the lack of leads that can be seen in the lead detection map (Fig. 6d). The absence of leads is therefore the main driver of the CS-2 freeboard and thickness uncertainty in areas of extended land-fast ice regions. However we do acknowledge that the assumption of uncorrelated uncertainties and thus the reduction by averaging might be an insufficient description of certain factors. For example the uncertainty of sea-surface anomaly can only be reduced by gridding if enough lead detections exist. If none are available within one grid cell, the uncertainty contribution due to the lack of leads would be constant for all CS-2 data points and not reduced by gridding. Also temporal variations are not included within one month, which might be significant during freeze-up and summer melt and result in visible orbit-patterns in the monthly means. The temporal and spatial covariances between uncertainty contributions of freeboard and thickness retrievals are only weakly constrained by observations, mainly in Arctic spring, and thus we have limited our uncertainty estimation to a first-order level. But the magnitude of uncertainty

TCD
8, 1831–1871, 2014

in the sea-ice thickness retrievals is in the order of direct comparisons between CS-2 data and airborne and moored validation data (Laxon et al., 2013).

The comparison of freeboard retrievals from the different applied retracker reveals that despite variable thresholds the mean geographical pattern is preserved. But the mean values vary with changing the threshold as a result of the different retrack positions (Fig. 3).

In contrast to TFMRA50 and TFMRA80, we assume a partial penetration for the TFMRA40 freeboard and thickness retrieval. The nature of the penetration parametrization (Eq. 5) has a significant effect on the thickness retrieval. While the modified W99 snow depth rarely exceeds the value for P_{max} over FYI, the parametrization generates only a partial radar penetration of the snow load over MYI. This can lead to a lower ratio of MYI to FYI thickness compared to the assumption that the penetration is always equal to the snow depth which is done for TFMRA50 and TFMRA80. This is also visible in the ice volume calculations (Fig. 9) where we find similar volumes for TFMRA40 and TFMRA50 but different ratios between FYI and MYI volume. In this study we use a simple penetration parametrization which assumes temporal and spatial constant values which can bias the thickness result. Furthermore the modified W99 snow depth, depending on ice type classification, might be only valid for a certain period and limited area.

Considering the trends between 2011 and 2013 we find a decline of sea-ice volume in March, but an increase in November. This counts for all applied thresholds and only differs in magnitude. Especially in November 2013 we observe a major increase of radar freeboard in the MYI region north of Greenland and the Canadian Archipelago compared to previous November data and even March 2013 in freeboard maps of all thresholds. This can be considered as unlikely since March represents the end of the winter season and November a period shortly after beginning of the freeze up. We can speculate that this an effect of a higher than usual snow load in combination with a limited penetration of the main scattering surface into the snow due to non negligible volume scattering caused by ice lenses and possibly wet snow in the beginning of the

TCD
8, 1831–1871, 2014

freezing season. This further implies that retracker with 50 % and also a 80 % threshold are not penetrating the snow completely in these conditions, which was assumed by Laxon et al. (2013) and Kurtz et al. (2014). This coincides with recent work by Willatt et al. (2010) and Willatt et al. (2011). They show that the CS-2 range estimates may only partially penetrate into the snow layer, thus a penetration correction would be required. Their findings are based on controlled ground-based K_u-Band radar experiments and aircraft validation data such as from the CryoSat-2 Validation Experiment (CryoVEx, see also Sect. 3).

Thus we can speculate how to accommodate the spatial and temporal variability of radar penetration in regions or periods where snow conditions can not be considered as cold and dry without significant internal density contrast by ice lenses. In these scenarios where the main scattering horizon is not penetrating the snow load completely the usage of a low-threshold retracker, avoiding volume scattering, might be reasonable to track the snow freeboard. On the other hand, in case of regions where penetration is physically possible, a high-threshold retracker might be the better choice. It would include volume scattering and thus track the ice freeboard. Such a parametrization is hypothetically at the moment and may result in significant biases if the choice of threshold is not correctly timed with the actual snow conditions.

We note that due to the uncertainties which arise from the freeboard to thickness conversion, the absolute volume of Arctic sea-ice is constrained to an uncertainty of ± 2 to $\pm 3 \times 10^3$ km^3, resulting from our uncertainty estimates. They are not including the potential uncertainties that arise due to the choice of the retracker. Considering the ice/radar freeboard, the choice of the retracker threshold in combination with the assumed penetration has a significant influence on the final retrieval. Nevertheless the threshold choice mostly affects the magnitude of ice/radar freeboard and the higher level products while the main trends remain.

TCD
8, 1831–1871, 2014

6 Conclusions

In this study we calculate CryoSat-2 radar freeboard and thickness retrievals with the first consistent uncertainty estimates in spring/autumn 2011, 2012 and 2013, applying three different thresholds for the threshold first-maximum retracker algorithm (TFMRA). The choice of the thresholds is based on current approaches by different scientific groups for CryoSat-2 data processing on Arctic sea-ice. In general the application of all thresholds gives confidence that the freeboard retrieval represents the actual distribution of sea-ice types. This is shown by direct comparisons with airborne laser altimetry on a local scale as well as with ASCAT backscatter data on a basin scale.

Our first-order uncertainty estimates have magnitudes comparable to those obtained through direct comparisons between CryoSat-2 data and validation datasets from aircraft and moorings (Laxon et al., 2013). The main driver of their geographical pattern are uncertainties in the sea-surface anomaly due to absence of leads and the density of CryoSat-2 ground tracks, in particular for the gridded products. This causes uncertainty patterns with a latitude-dependent gradient and increased uncertainties in areas with a lack of leads like land-fast-ice regions, e.g. Laptev Sea.

The choice of retracker thresholds mostly change the magnitude of the freeboard and higher level products like sea-ice thickness and volume. We find declines of Arctic sea-ice volumes of 9.7 % (TFMRA40), 10.9 % (TFMRA50) and 6.9 % (TFMRA80) between March 2011 and 2013. In contrast to that we find increases in Arctic sea-ice volume of 27.88 % (TFMRA40), 25.71 % (TFMRA50) and 32.65 % (TFMRA80) from November 2011 to 2013. seasonal bias This strong rise of volume in November should be in the focus of future investigation, also because the comparison between March and November 2013 retrievals shows an increase of radar freeboard in the MYI region north of Greenland and the Canadian Archipelago from March to November which is unlikely. It gives rise to the assumption that even by applying an 80 % threshold retracker (TFMRA80) the radar does not penetrate through the snow load completely.

TCD
8, 1831–1871, 2014

Therefore we can anticipate a seasonal bias in the CryoSat-2 freeboard retrieval and higher level products.

Thus, for the future it would be useful to investigate different thresholds depending on the properties of the snow load e.g. seasonal or location specific retrackers. To support this there is a strong need for more information and measurements on the spatial and temporal variability of snow properties.

Acknowledgements. The validation measurements in the framework of CryoVEx and PAMARCMIP 2011 campaigns were carried out by the DTU Space and the Alfred Wegener Institute, Helmholtz Centre for Polar and Marine Research, Bremerhaven, Germany. The CryoVEx campaigns are part of ESA's Living Planet Program. The CryoSat-2 data are provided by the European Space Agency. All this is gratefully acknowledged.

References

Alexandrov, V., Sandven, S., Wahlin, J., and Johannessen, O. M.: The relation between sea ice thickness and freeboard in the Arctic, The Cryosphere, 4, 373–380, doi:10.5194/tc-4-373-2010, 2010. 1841, 1860

Andersen, O. B.: The DTU10 Gravity field and Mean sea surface, second international symposium of the gravity field of the Earth (IGFS2), Fairbanks, Alaska, 20–22 September 2010, 2010. 1837

Beaven, S. G., Lockhart, G. L., Gogineni, S. P., Hossetnmostafa, A. R., Jezek, K., Gow, A. J., Perovich, D. K., Fung, A. K., and Tjuatja, S.: Laboratory measurements of radar backscatter from bare and snow-covered saline ice sheets, Int. J. Remote Sens., 16, 851–876, doi:10.1080/01431169508954448, 1995. 1834

Brodzik, M. J., Billingsley, B., Haran, T., Raup, B., and Savoie, M. H.: EASE-Grid 2.0: incremental but significant improvements for earth-gridded data sets, ISPRS Int. J. Geo-Inf. 2012, 1, 32–45, doi:10.3390/ijgi1010032, 2012. 1842

Comiso, J. C., Parkinson, C. L., Gersten, R., and Stock, L.: Accelerated decline in the Arctic sea ice cover, Geophys. Res. Lett., 35, L01703, doi:10.1029/2007GL031972, 2008. 1833

TCD
8, 1831–1871, 2014

Drinkwater, M. R.: Ku band airborne radar altimeter observations of marginal sea ice during the 1984 Marginal Ice Zone Experiment, J. Geophys. Res.-Oceans, 96, 4555–4572, doi:10.1029/90JC01954, 1991. 1837

Eastwood, S.: OSI SAF Sea Ice Product Manual, v3.8 edn., available at: http://osisaf.met.no (last access: 10 January 2014), 2012. 1838, 1841

Forsberg, R., Keller, K., and Jacobsen, S.: Airborne lidar measurements for Cryosat validation, in: Geoscience and Remote Sensing Symposium, 2002. IGARSS '02. 2002 IEEE International, 24–28 June, Toronto, Canada, vol. 3, 1756–1758, doi:10.1109/IGARSS.2002.1026244, 2002. 1846

Giles, K., Laxon, S., Wingham, D., Wallis, D., Krabill, W., Leuschen, C., McAdoo, D., Manizade, S., and Raney, R.: Combined airborne laser and radar altimeter measurements over the Fram Strait in May 2002, Remote Sens. Environ., 111, 182–194, doi:10.1016/j.rse.2007.02.037, remote Sensing of the Cryosphere Special Issue, available at: http://www.sciencedirect.com/science/article/pii/S0034425707002817 (last access: 28 March 2014), 2007. 1844

Giles, K. A., Laxon, S. W., and Ridout, A. L.: Circumpolar thinning of Arctic sea ice following the 2007 record ice extent minimum, Geophys. Res. Lett., 35, L22502, doi:10.1029/2008GL035710, 2008. 1837

Helm, V., Humbert, A., and Miller, H.: Elevation and elevation change of Greenland and Antarctica derived from CryoSat-2, The Cryosphere Discuss., 8, 1673–1721, doi:10.5194/tcd-8-1673-2014, 2014. 1834, 1836

Kurtz, N. T. and Farrell, S. L.: Large-scale surveys of snow depth on Arctic sea ice from Operation IceBridge, Geophys. Res. Lett., 38, L20505, doi:10.1029/2011GL049216, 2011. 1841

Kurtz, N. T., Farrell, S. L., Studinger, M., Galin, N., Harbeck, J. P., Lindsay, R., Onana, V. D., Panzer, B., and Sonntag, J. G.: Sea ice thickness, freeboard, and snow depth products from Operation IceBridge airborne data, The Cryosphere, 7, 1035–1056, doi:10.5194/tc-7-1035-2013, 2013. 1844

Kurtz, N. T., Galin, N., and Studinger, M.: An improved CryoSat-2 sea ice freeboard and thickness retrieval algorithm through the use of waveform fitting, The Cryosphere Discuss., 8, 721–768, doi:10.5194/tcd-8-721-2014, 2014. 1834, 1835, 1836, 1837, 1839, 1853

Kwok, R., Cunningham, G. F., Wensnahan, M., Rigor, I., Zwally, H. J., and Yi, D.: Thinning and volume loss of the Arctic Ocean sea ice cover: 2003–2008, J. Geophys. Res., 114, C07005, doi:10.1029/2009JC005312, 2009. 1833

TCD
8, 1831–1871, 2014

Laxon, S.: Sea ice altimeter processing scheme at the EODC, Int. J. Remote Sens., 15, 915–924, doi:10.1080/01431169408954124, 1994. 1837

Laxon, S., Peacock, N., and Smith, D.: High interannual variability of sea ice thickness in the Arctic region, Nature, 425, 947–950, 2003. 1833, 1834

Laxon, S. W., Giles, K. A., Ridout, A. L., Wingham, D. J., Willatt, R., Cullen, R., Kwok, R., Schweiger, A., Zhang, J., Haas, C., Hendricks, S., Krishfield, R., Kurtz, N., Farrell, S., and Davidson, M.: CryoSat-2 estimates of Arctic sea ice thickness and volume, Geophys. Res. Lett., 40, 732–737, doi:10.1002/grl.50193, 2013. 1833, 1834, 1835, 1837, 1838, 1839, 1841, 1843, 1852, 1853, 1854

Matzler, C. and Wegmuller, U.: Dielectric properties of freshwater ice at microwave frequencies, J. Phys. D Appl. Phys., 20, 1623–1630, doi:10.1088/0022-3727/20/12/013, 1987. 1839

Nghiem, S. V., Rigor, I. G., Perovich, D. K., Clemente-Colón, P., Weatherly, J. W., and Neumann, G.: Rapid reduction of Arctic perennial sea ice, Geophys. Res. Lett., 34, L19504, doi:10.1029/2007GL031138, 2007. 1841

Peacock, N. R. and Laxon, S. W.: Sea surface height determination in the Arctic Ocean from ERS altimetry, J. Geophys. Res.-Oceans, 109, C07001, doi:10.1029/2001JC001026, 2004. 1837

Rothrock, D. A., Yu, Y., and Maykut, G. A.: Thinning of the Arctic sea-ice cover, Geophys. Res. Lett., 26, 3469–3472, doi:10.1029/1999GL010863, 1999. 1833

Stroeve, J., Serreze, M., Holland, M., Kay, J., Malanik, J., and Barrett, A.: The Arctic's rapidly shrinking sea ice cover: a research synthesis, Climatic Change, 110, 1005–1027, doi:10.1007/s10584-011-0101-1, 2012. 1833

Wadhams, P., Tucker, W. B. I., Krabill, W. B., Swift, R. N., Comiso, J. C., and Davis, N. R.: Relationship between sea ice freeboard and draft in the Arctic Basin, and implications for ice thickness monitoring, J. Geophys. Res., 97, 20325–20334, doi:10.1029/92JC02014, 1992. 1834

Warren, S. G., Rigor, I. G., Untersteiner, N., Radionov, V. F., Bryazgin, N. N., Aleksandrov, Y. I., and Colony, R.: Snow Depth on Arctic Sea Ice, J. Climate, 12, 1814–1829, doi:10.1175/1520-0442(1999)012<1814:SDOASI>2.0.CO;2, 1999. 1841, 1860

Willatt, R., Giles, K., Laxon, S., Stone-Drake, L., and Worby, A.: Field investigations of Ku-band radar penetration into snow cover on Antarctic Sea ice, IEEE T. Geosci. Remote, 48, 365–372, doi:10.1109/TGRS.2009.2028237, 2010. 1853

TCD
8, 1831–1871, 2014

Willatt, R., Laxon, S., Giles, K., Cullen, R., Haas, C., and Helm, V.: Ku-band radar penetration into snow cover on Arctic sea ice using airborne data, Ann. Glaciol., 52, 197–205, 2011. 1834, 1853

Wingham, D. J., Francis, C. R., Baker, S., Bouzinac, C., Brockley, D., Cullen, R., de Chateau-Thierry, P., Laxon, S. W., Mallow, U., Mavrocordatos, C., Phalippou, L., Ratier, G., Rey, L., Rostan, F., Viau, P., and Wallis, D. W.: CryoSat: a mission to determine the fluctuations in Earth's land and marine ice fields, Adv. Space Res., 37, 841–871, doi:10.1016/j.asr.2005.07.027, 2006. 1838, 1842, 1843, 1860

Wingham, D. J., Rapley, C. G., and Griffiths, H.: New techniques in satellite altimeter tracking systems, in: Proceedings of the IGARSS Symposium, Zurich, Switzerland, 8–11 Sepember 1986, edited by: Guyenne, T. and Hunt, J., vol. SP-254, European Space Agency, 1339–1344, 1986. 1838

Wingham, D., Phalippou, L., Mavrocordatos, C., and Wallis, D.: The mean echo and echo cross product from a beamforming interferometric altimeter and their application to elevation measurement, IEEE T. Geosci. Remote Sens., 42, 2305–2323, doi:10.1109/TGRS.2004.834352, 2004. 1834

TCD
8, 1831–1871, 2014

Table 1. Waveform parameter and ice concentration thresholds used in the CryoSat-2 processing algorithm to discriminate between the surface types "Ocean", "Lead" and "Sea ice": pulse peakiness PP, stack kurtosis K, standard deviation SSD, peakiness PP_l left of the power maximum, peakiness PP_r right of the power maximum, sea-ice concentration IC and the width of the OCOG box (OCOG WIDTH).

	Waveform parameter						
Type	PP	K	SSD	PP_l	PP_r	IC (%)	OCOG WIDTH
Ocean	$0 \leq PP \leq 10$		≥ 18.5			≤ 5	≥ 38
Lead	≥ 40	≥ 40	≤ 4	≥ 40	≥ 30	≥ 70	
Sea ice		≤ 8			≤ 15	≥ 70	

TCD
8, 1831–1871, 2014

Table 2. Estimations of the individual uncertainties which contribute to the calculations in Eqs. (10) and (11): uncertainties of snow depth (σ_Z), radar freeboard (σ_{F_R}), radar penetration (σ_P), sea-surface anomaly (σ_{SSA}), speckle noise (σ_{l1b}), ice density (σ_{ρ_I}) and snow density (σ_{ρ_S}).

Parameter	Value	Reference/source
σ_Z	Variable	Warren et al. (1999)
σ_{F_R}	Variable	Radar freeboard uncertainty, Eq. (10)
σ_P	0.1 m	Measurements, CryoVex 2011
σ_{SSA}	Variable	Depending on lead coverage
σ_{l1b}	0.10–0.14 m	Wingham et al. (2006)
σ_{ρ_I}	FYI: 35.7 kg m^{-3}	Alexandrov et al. (2010)
	MYI: 23 kg m^{-3}	
σ_{ρ_S}	100.0 kg m^{-3}	Estimation based on Warren et al. (1999)

TCD
8, 1831–1871, 2014

Table 3. Mean radar and ice freeboard F_R, F_I and sea-ice thickness estimates T of gridded data for March and November 2013, corresponding to Figs. 7 and 8, discriminated between first-year ice (FYI) and multi-year ice (MYI).

	March 2013				November 2013			
	FYI		MYI		FYI		MYI	
	F_R (m)	T (m)	F_R (m)	T (m)	F_R (m)	T (m)	F_R (m)	T (m)
TFMRA40	0.17	1.97	0.30	2.10	0.11	1.25	0.31	2.22
	F_I (m)		F_I (m)		F_I (m)		F_I (m)	
TFMRA50	0.14	1.71	0.28	2.74	0.09	1.02	0.26	2.34
TFMRA80	0.09	1.16	0.18	1.88	0.06	0.64	0.15	1.43

TCD
8, 1831–1871, 2014

Table 4. Arctic volumes V of March and November 2011 are used as a reference to calculate differences ΔV from the same month in the following years, also given as fraction f of the 2011 retrieval. This is done for the TFMRA retracker thresholds 40 % (TFMRA40), 50 % (TFMRA50) and 80 % (TFMRA80). Absolute volume uncertainties σ_V are estimated following Eq. (13). Uncertainties of volume differences $\sigma_{\Delta V}$ are obtained by adding of the individual uncertainty contributions.

		TFMRA40			TFMRA50			TFMRA80		
		V (10^3 km^3)	f (%)	σ_V (10^3 km^3)	V (10^3 km^3)	f (%)	σ_V (10^3 km^3)	V (10^3 km^3)	f (%)	σ_V (10^3 km^3)
2011	Mar	16.27		2.57	16.21		2.70	10.59		3.05
	Nov	9.04		2.04	8.63		2.11	5.20		2.33
		ΔV		$\sigma_{\Delta V}$	ΔV		$\sigma_{\Delta V}$	ΔV		$\sigma_{\Delta V}$
2012	Mar	−1.32	−8.12	4.89	−1.78	−11.36	5.19	−1.08	−10.19	6.18
	Nov	0.71	7.89	3.85	0.50	1.11	3.98	0.28	5.38	4.36
2013	Mar	−1.57	−9.67	4.58	−1.69	−10.86	4.82	−0.73	−6.91	5.51
	Nov	2.52	27.88	4.11	2.62	25.71	4.28	1.70	32.65	4.79

TCD
8, 1831–1871, 2014

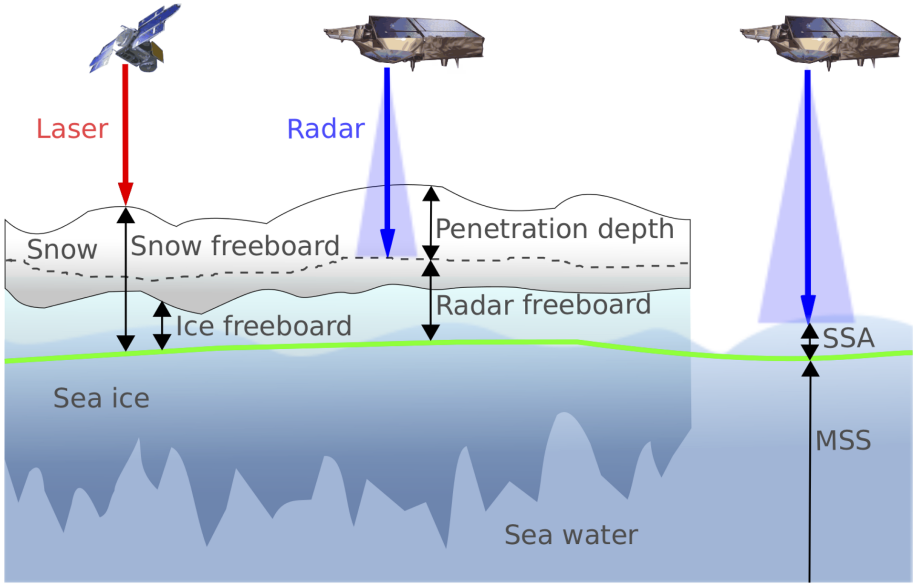

Fig. 1. Schematic diagram of parameter regarding the CryoSat-2 freeboard and thickness processing. The actual sea-surface height is composed of the mean sea-surface height (MSS) and the sea-surface anomaly (SSA). The radar freeboard is obtained by subtracting the actual sea surface from the range retrieval over sea-ice. In contrast to a laser altimeter (e. g. IceSat), the radar altimeter of CryoSat-2 can penetrate the snow cover, depending on the snow properties.

TCD
8, 1831–1871, 2014

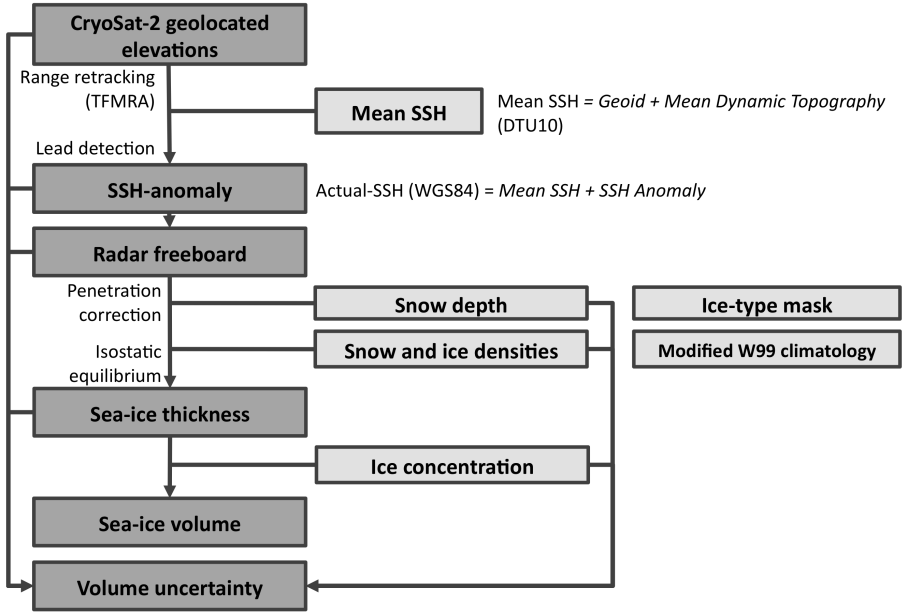

Fig. 2. Flowchart of the CryoSat-2 data processing algorithm.

TCD
8, 1831–1871, 2014

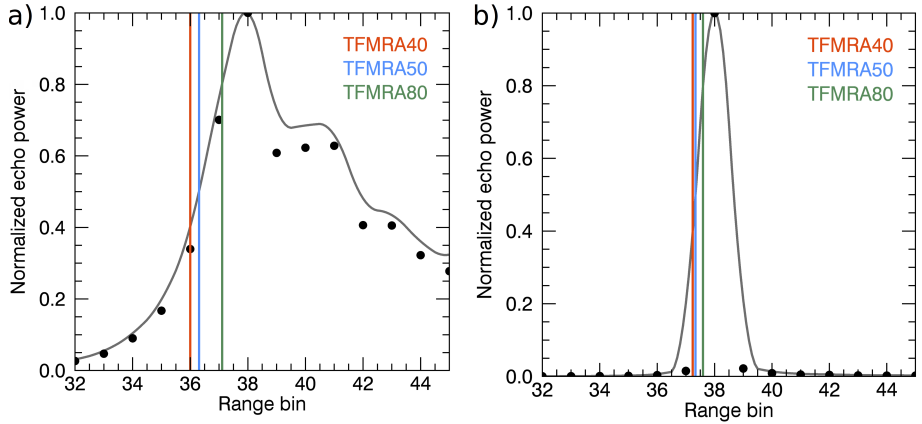

Fig. 3. Exemplary extractions of CryoSat-2 waveforms for sea-ice **(a)** and leads **(b)**. The fitted waveform (grey) is a result of linear interpolation and smoothing of the original CryoSat-2 waveform (black dots). The colored vertical lines represent the different applied TFMRA (Threshold first-maximum retracker algorithm) thresholds in this study: 40 % (TFMRA40), 50 % (TFMRA50) and 80 % (TFMRA80).

TCD
8, 1831–1871, 2014

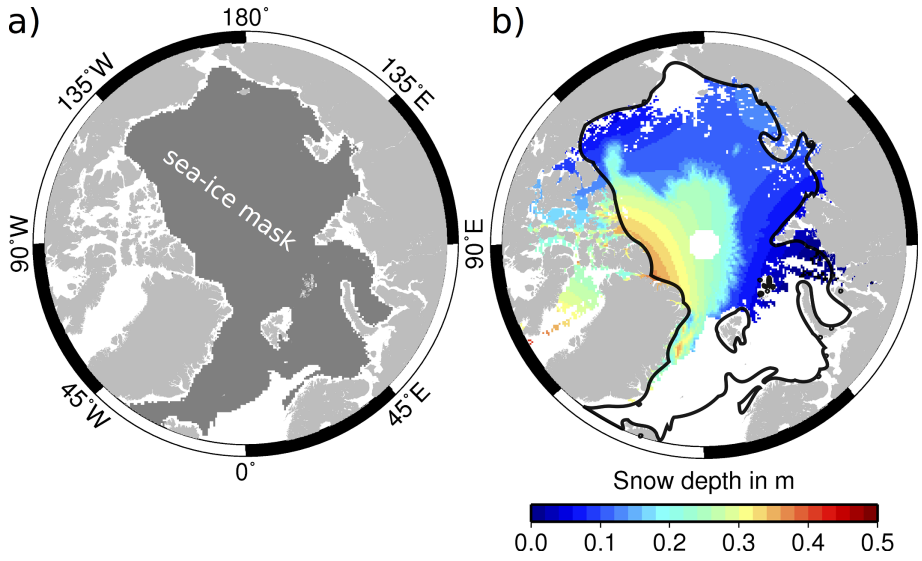

Fig. 4. (a) Data mask, which is applied to the thickness retrieval to calculate monthly volume estimates. Only thickness data within the dark grey area are used for the calculation of the volume estimates. **(b)** Exemplary snow depth of November 2011 overlaid by the data mask (solid black line). Thickness data in excluded regions are discarded because the W99 snow depth fit is not valid there.

TCD
8, 1831–1871, 2014

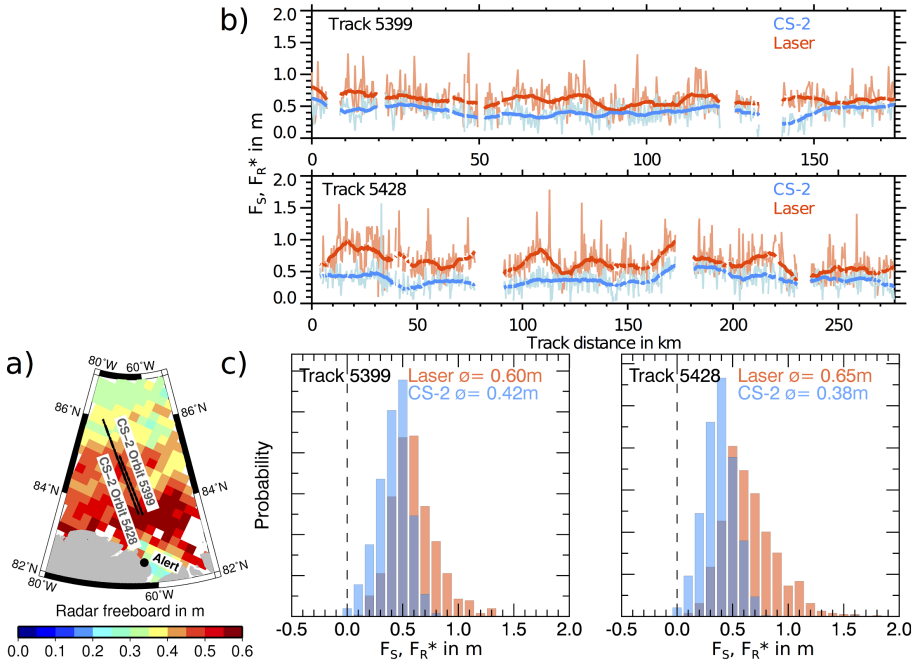

Fig. 5. (a) Area of coincident flights of CryoSat-2 and Polar-5 (black box in Fig. 6) from 15 and 17 April 2011. The aircraft surveyed the ascending CryoSat-2tracks from the South East to the North West. **(b)** Uncorrected TFMRA40 radar freeboard (F_R^*) of CryoSat-2 and snow freeboard (F_S) from airborne laser altimetry (Laser) along CryoSat-2 tracks 5399 and 5428. **(c)** Probability density functions of F_R^* and F_S. For the comparison only valid data from coincident coverage are considered.

TCD
8, 1831–1871, 2014
CryoSat-2
R. Ricker et al.

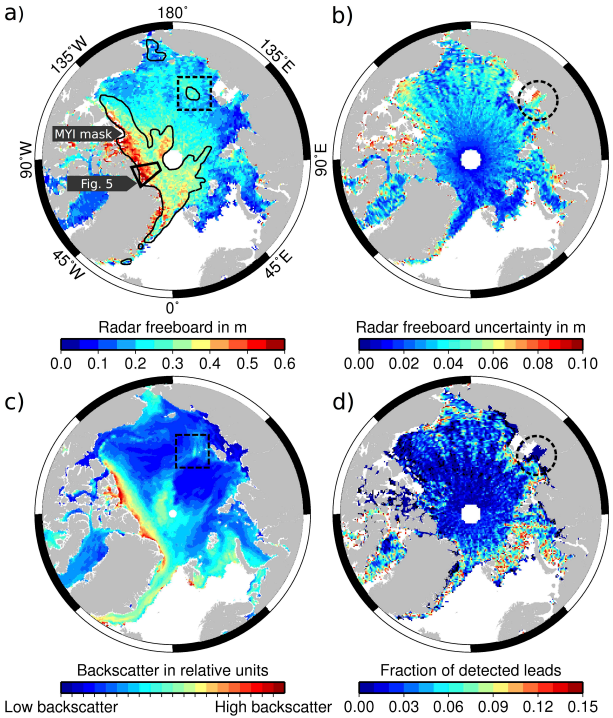

Fig. 6. (a) CryoSat-2 mean radar freeboard of April 2011, retrieved by applying the TFMRA40 retracker. It shows the area of coincident validation flights in April 2011 (black box, see Fig. 5). The dashed black dashed box marks a common feature of **(a)** and **(c)**. **(b)** Corresponding uncertainties of the radar freeboard. **(c)** METOP ASCAT mean backscatter for 04/2011. **(d)** Detected leads as fraction of the total number of CryoSat-2 point measurements within one grid cell. The dashed circle marks a land-fast ice region with low density of leads, resulting in an increased uncertainty.

TCD
8, 1831–1871, 2014

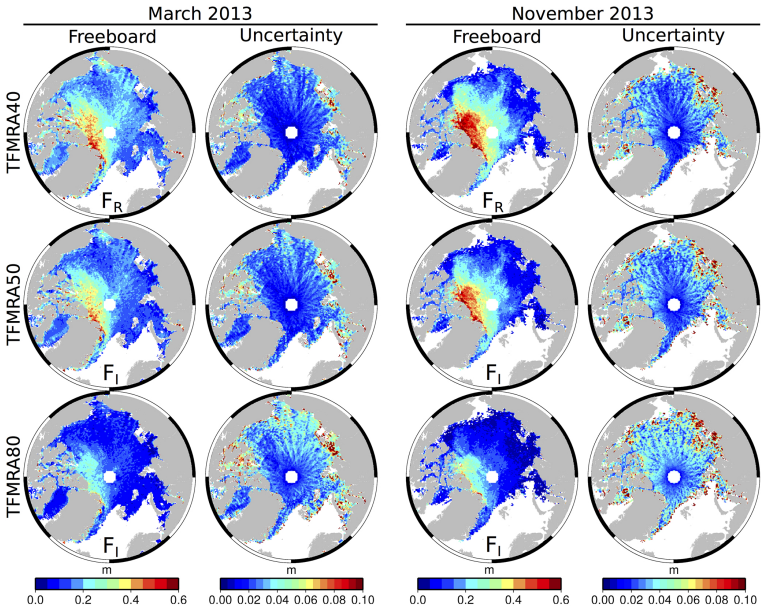

Fig. 7. CryoSat-2 freeboard retrieval with uncertainties of March and November 2013. The freeboard processing is accomplished applying three different TFMRA (Threshold first-maximum retracker algorithm) retracker thresholds: 40 % (TFMRA40), 50 % (TFMRA50) and 80 % (TFMRA80). Furthermore for TFMRA40 we assume the radar freeboard F_R as a result of a penetration of 0.18 m into snow, while for TFMRA50 and TFMRA80 we assume the freeboard to be equal to the ice freeboard F_I.

TCD
8, 1831–1871, 2014

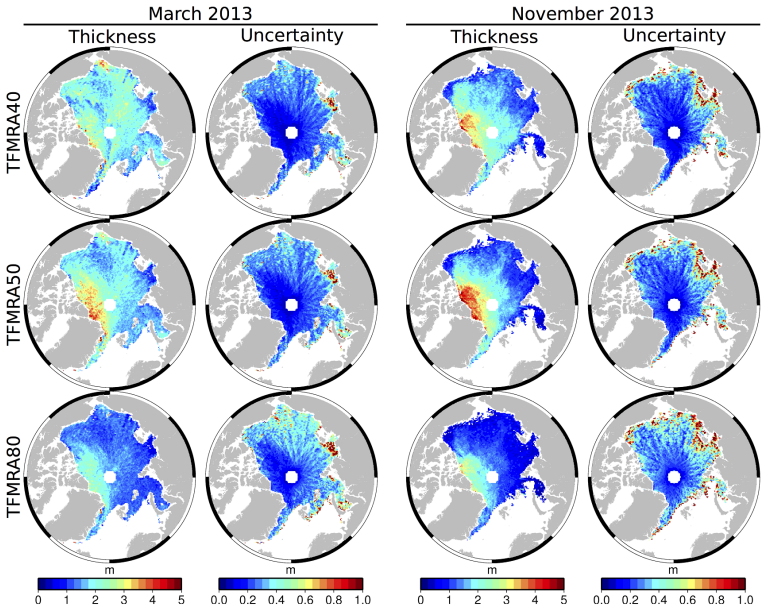

Fig. 8. CryoSat-2 sea-ice thickness retrieval with uncertainties of March and November 2013. The thickness processing is accomplished applying three different TFMRA (Threshold first-maximum retracker algorithm) retracker thresholds: 40 % (TFMRA40), 50 % (TFMRA50) and 80 % (TFMRA80). Furthermore we assume a maximum radar penetration of 0.18 for the free-board to thickness conversion, while for TFMRA50 and TFMRA80 we assume the penetration to be equal to the snow depth (see also Fig. 7).

TCD
8, 1831–1871, 2014

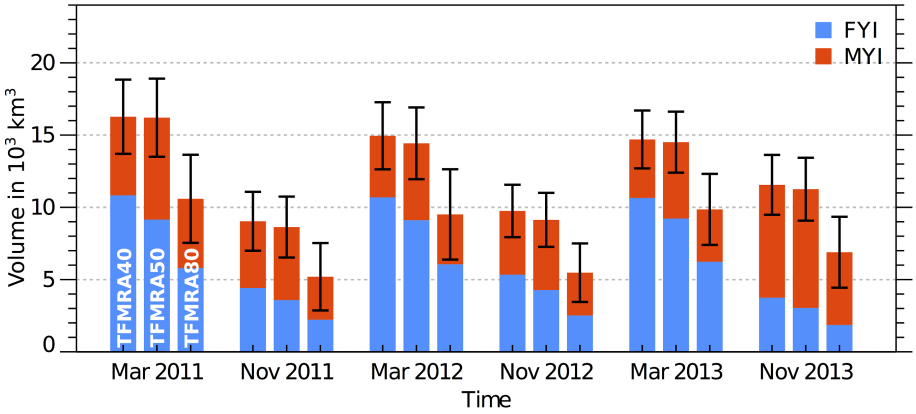

Fig. 9. Arctic sea-ice volume of March and November 2011–2013 after applying TFMRA (Threshold first-maximum retracker algorithm) retracker thresholds 40 % (TFMRA40), 50 % (TFMRA50) and 80 % (TFMRA80) of the power of the first maximum of the waveforms, discriminated between first-year ice (FYI) and multi-year ice (MYI).

TCD
8, 1831–1871, 2014